Light-Induced Electron Spin Polarization in Vanadyl Octaethylporphyrin: I. Characterization of the Excited Quartet State

Yuri E. Kandrashkin,[†,‡] Motoko S. Asano,[§,||] and Art van der Est*[,†]

Department of Chemistry, Brock University, 500 Glenridge Ave. St. Catharines Onterio, Canada L2S 3A1, Kazan Physical-Technical Institute Russian Academy of Sciences, Kazan, Russian Federation, and Department of Chemistry, Tokyo Institute of Technology, O-okayama, Meguro-ku, Tokyo 152-8551, Japan

Received: April 2, 2006; In Final Form: June 6, 2006

Laser flash induced spin-polarized transient electron paramagnetic resonance (TREPR) spectra for vanadyl octaethylporphyrin in isotropic and partially ordered frozen solutions are presented and compared with corresponding luminescence data. The TREPR spectra show well-resolved hyperfine couplings to the vanadium nucleus and a multiplet polarization pattern with features typical of zero-field splitting (ZFS). The principal values of the vanadium hyperfine coupling tensor evaluated from the spectra are 1/3 of the corresponding values found from steady-state EPR spectra of the ground state. On the basis of these characteristics and numerical simulations, the polarization patterns are assigned to the excited quartet state. The values of the ZFS parameters of the trip-quartet obtained from simulation of the spectra ($D = 17.5$ mT and $E = 1.5$ mT) are comparable to those of the triplet state of the zinc and free base octaethyl porphyrin. The lifetime of the spin polarization is found to be temperature dependent and is essentially the same as that of the optical emission. The temperature dependence is rationalized using a model in which the decay to the ground state occurs from both the trip-quartet and trip-doublet, which are in thermal equilibrium even at 15 K. A fit of the model to the observed spin polarization lifetimes yields an energy gap of 47 cm^{-1} between the trip-quartet and trip-doublet. It is shown that the spin polarization evolves from a multiplet pattern at early times to a net absorptive pattern at late times following the laser flash. It is proposed that the establishment of thermal equilibrium leads to the evolution of the spin from multiplet to net polarization.

1. Introduction

Porphyrins and their derivatives play essential roles in nature, mostly due to their ability to bind a wide variety of metals and to become chemically active upon light excitation. This combination of properties makes them ideal as building blocks for complexes designed to capture and store light energy (see refs 1−6 for some recent examples). One of the challenges encountered in designing such systems is the need to control the photochemistry of the porphyrin in the presence of metal ions, which have a variety of electronic structures. In the case of paramagnetic metalloporphyrins, the magnetic and/or electronic interactions between the central metal and the porphyrin π-system have a profound impact on the nature of the excited states and the photodynamics of the whole system. Hence, a detailed understanding of these interactions and their influence on the excited-state dynamics is central to the design of metalloporphyrin-based supramolecular complexes.

In Figure 1, a Jablonski diagram of a molecule, in which the π−electron system and a single *d*-electron are combined, is presented using vanadyl octaethylporphyrin as an example. The presence of the unpaired electron on the central metal means that the ground state and singlet excitations of the porphyrin π-electrons are doublet states, whereas the exchange interaction splits the triplet excitations of the porphyrin into doublet and quartet states. Using the notation first introduced by Gouterman,[7,8] these states are usually referred to as "sing-doublet", "trip-doublet", and "trip-quartet" and are given the symbols ^{2}S, ^{2}T, and ^{4}T, respectively. The terms "sing" or "trip" and the corresponding symbols S or T describe the spin state of the π-electrons, which in general are coupled most strongly. The terms doublet and quartet and the corresponding superscript express the entire spin multiplicity of the state. We assume that the lowest excited state is the trip-quartet,[8] as predicted theoretically[7] and observed in copper porphyrins.[9−12] (Note that the separation of the energy levels in Figure 1 is not to scale and is only meant to give a qualitative picture of the relative energies.) For octaalkyl porphyrins, the $a_{1u} \rightarrow e_g$ excitation is predicted to be of lowest energy,[9,13,14] giving a doubly degenerate excited state of E_u symmetry.[7−9] The peripheral substituents and surroundings are expected to lift the degeneracy of the E_u state,[15,16] resulting in two low-lying trip-doublet and trip-quartet states. The states are labeled (a_1e_x) and (a_1e_y) according to the orientation in the molecular plane of the transition dipole moments associated with the excitation. (Note that vanadyl porphyrins have C_{4v} symmetry; hence, the states are labeled a_1e and not $a_{1u}e_g$ as they would be for a metalloporphyrin with D_{4h} symmetry.)

Following light absorption and relaxation to the lowest excited sing-doublet state $^2S_1$, rapid decay to the lowest trip-doublet state, $^2T_1$, can occur because it acquires some sing-doublet character due to the different exchange interactions of the two unpaired π-electrons with the *d*-electron of the metal.[9,15]

* To whom correspondence should be addressed. E-mail: avde@brocku.ca. FAX: 905-682-9020.
† Brock University.
‡ Kazan Physical−Technical Institute Russian Academy of Sciences.
§ Tokyo Institute of Technology.
|| Current address: Department of Chemistry, Graduate School of Science and Engineering, Tokyo Metropolitan University 1−1, Minami-Ohsawa, Hachi-Ohji,Tokyo 192-0397, Japan.

10.1021/jp0620365 CCC: $33.50 © 2006 American Chemical Society
Published on Web 07/19/2006

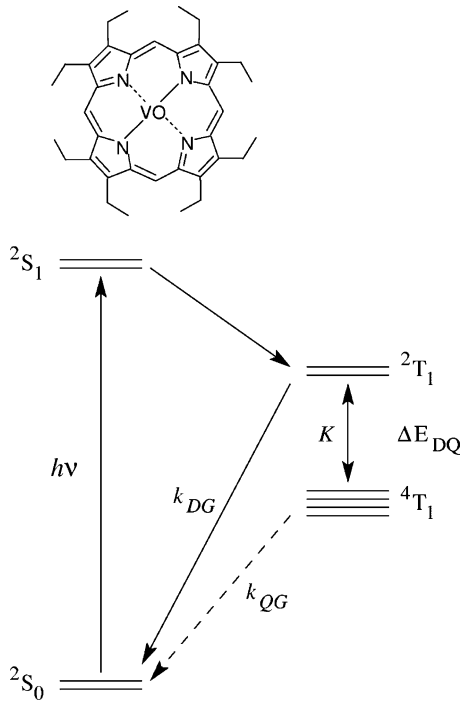

Figure 1. Molecular structure of vanadyl octaethylporphyrin and simplified Jablonski diagram. The states are labeled according to the overall spin as a superscript (2 = doublet, 4 = quartet) and the electronic configuration of the porphyrin $\pi-$orbitals (S = singlet, T = triplet). Following light absorption to the excited sing-doublet state, ($^2S_1$) decays to the trip-doublet manifold ($^2T_1$) and then to the lowest trip-quartet state ($^4T_1$). Relaxation to the ground state is proposed to occur primarily from the trip-doublet state populated via thermal equilibrium from the trip-quartet. The decay rates from the trip-doublet and trip-quartet to the ground state are k_{DG} and k_{QG}, respectively. The equilibrium between the trip-doublet and trip-quartet is governed by the equilibrium constant, *K*.

Subsequent intersystem crossing from the trip-doublet to the trip-quartet, $^4T_1$, is also highly efficient as shown by picosecond and femtosecond absorption spectroscopy studies of copper porphyrins.[17−19] The decay of the trip-quartet to the ground state can follow several pathways. The direct path, governed by k_{QG} (see Figure 1), is slow. Hence, at sufficiently high temperature, decay via the trip-doublet, which has a faster rate, k_{DG}, is also possible. Which of these two pathways is favoured depends critically on the energy gap between the trip-doublet and trip-quartet, ΔE_{DQ}, and the temperature. If ΔE_{DQ} is relatively small compared to kT, thermal equilibration of the trip-quartet and trip-doublet can occur as indicated by the double-headed arrow between them in Figure 1, and both states will have the same lifetime. However, because the decay rate from the trip-doublet k_{DG} is expected to be greater than that from the trip-quartet, k_{QG}, the emission observed at ambient temperatures is ascribed to radiative decay from the trip-doublet.[8,9,17,20]

Time-resolved optical spectroscopy in its various forms provides a good method for monitoring the excited-state kinetics of such complexes.[21] However, it has the disadvantage that it can be difficult to distinguish nearly degenerate states of different multiplicity, which can be crucial for the photochemistry. Because of this, considerable effort has been invested in trying to observe the excited multiplet states of such systems by magnetic resonance techniques,[16,22] in particular time-resolved electron paramagnetic resonance (EPR) spectroscopy.[23] These states are expected to show enhanced electron spin polarization that, together with the magnetic parameters (zero-field splitting, hyperfine couplings, g-tensor), provides detailed information about the dynamics and the electronic structure of the system.

However, attempts to measure spin-polarized EPR signals of the excited states of monomeric paramagnetic metalloporphyrins themselves have been largely unsuccessful. In water-soluble copper porphyrins[24] and self-assembled electrostatic porphyrin dimers,[25] the observed polarization was assigned to the ground state, and it was proposed that it resulted from transfer of the net component of the trip-quartet polarization during electronic relaxation. A Cr(V)O−corrole also showed spin polarization,[26] which was likewise assigned to the ground state. A broad, featureless, emissive spectrum of a Co(II) porphyrin ligated by oxygen was briefly mentioned by Yamauchi,[23] but apart from this spectrum, spin-polarized EPR data from the excited multiplet states of paramagnetic porphyrins are conspicuously absent in the literature. On the other hand, the excited multiplet states of complexes containing one or more stable radicals tethered to an otherwise diamagnetic chromophore such as a porphyrin or C_{60} have been observed,[27−44] and we have also reported spin-polarized EPR spectra of triplet−doublet spin pairs in covalently linked copper porphyrin−free-base porphyrin dimers.[45−47] It is likely that the difficulty in observing the excited states of paramagnetic metal complexes by transient EPR is related to the large zero-field splitting associated with the metal, which probably leads to very broad spectra with short spin−lattice relaxation times.

Based on the premise that such effects should be smaller in the light transition metals such as vanadium, we have begun a study of vanadyl porphyrins. Recently, we reported the first spin-polarized TREPR spectra of the excited states of a paramagnetic metal complex, using vanadyl octaethylporphyrin (OEPVO).[48] Here, we present a more detailed account of the TREPR data of OEPVO and the evidence supporting their assignment to the lowest trip-quartet state. We will show that the light-induced spin polarization has the same lifetime as the luminescence over a wide temperature range, and below ∼50 K, the TREPR spectra display a well-resolved hyperfine structure due to the $I = 7/2$ vanadium nucleus. Using a partially ordered liquid crystalline solvent, we are able to extract the principal values of the hyperfine tensor and show that they are one-third of the corresponding values in the ground state. Moreover, predominantly multiplet spin polarization is observed at early times. Together, these features lead to an assignment of the observed signals to the excited trip-quartet state. In addition, we will show that the TREPR spectrum of the trip-quartet state evolves to a pattern with pure net polarization at late times. We propose that the initial multiplet polarization is generated in the trip-quartet state by intersystem crossing (ISC) from the trip-doublet and that the net polarization is built up at the expense of the multiplet contribution by the subsequent equilibration of the trip-quartet and trip-doublet states. In the accompanying paper,[49] this proposal is explored in more detail with an analysis of the time dependence of the polarization and the development of a model describing the mechanism by which the net polarization evolves.

2. Experimental Section

Preparation of OEPVO. 2,3,7,8,12,13,17,18-octaethylporphynato oxovanadium(IV) (OEPVO) was prepared by refluxing the corresponding free base porphyrin in dimethylformamide for 40 h with an excess of vanadyl sulfate, which was added to the reaction mixture by two portions. The product was purified by chromatography on a dry-packed alumina column (Merck Alumium Oxide 90 (II−III)) and then of silica gel (Wakogel

C-200) with CH_2Cl_2 as eluent, mainly to separate unreacted free base porphyrin. Further purification was carried out by recrystallization from CH_2Cl_2/ethanol, and finally the crystals were washed by hexane and dried.

EPR Experiments. EPR samples were prepared by dissolving OEPVO in either toluene or the liquid crystalline solvent, E7 (Merck), to a concentration of $\sim 10^{-4}$ M. The solutions were placed in suprasil EPR sample tubes (4 mm o.d.) and were degassed by several freeze−pump−thaw cycles and then sealed under vacuum. The transient EPR (TREPR) measurements were performed at X-band (9 GHz) using a setup described previously.[50,51] Optical excitation at 532 nm was achieved using a Nd:YAG laser.

Optical Emission Spectra and Lifetimes. For the optical measurements at 77 K, a solution of OEPVO in toluene containing 5% polystyrene was sealed in a suprasil EPR tube as described above and placed in a quartz Dewar, filled with liquid nitrogen.

For other temperatures between 4 and 120 K, transparent films of OEPVO in poly(methyl methacrylate) (PMMA) were used. The commercially available PMMA (degree of polymerization 7000−7500) was purified three times by reprecipitation from CH_2Cl_2/methanol. The sample films were prepared by spontaneous evaporation of a homogeneous viscous solution of PMMA and porphyrin in CH_2Cl_2 on a clean glass plate covered with a Petri dish. For the measurements, the film was mounted in a Japan Thermal Engineering cryostat (Model JHCS-HK-4.2-005).

Emission spectra were recorded on a Hitachi 4500 spectrofluorimeter equipped with a Hamamatsu photonics R928 photomultiplier. For the lifetime measurements, the porphyrin solution was excited at 532 nm by a nanosecond Nd:YAG laser. Transient emission signals were observed through a Nikon P-250 monochromator by a R928 photomultiplier and were digitized and accumulated using a Leroy digital oscilloscope. The lifetimes were determined by fitting the decay curves using an iterative least-squares method.

EPR Spectral Simulations and Fitting. The spectral simulations and fitting were performed using a program based on the Mathematica system. The program models the stick spectra for a static spin-Hamiltonian in the linear response regime and exploits the ability of Mathematica to deal with analytical expressions. It also uses a package called Spin Algebra that we have developed, which allows all inputs to be made as spin operators in the traditional form described in magnetic resonance textbooks. The program also supports unlimited spin systems with arbitrary spin multiplicities. The calculation of the resonance frequencies and signal intensity along with the details of the integration method used for the powder average are given in Appendix 1. The orientational distribution function needed for the liquid crystal samples is described in Appendix 2.

3. Results

3.1. Spin Polarization and Fluorescence Decay at 80 K. The spin-polarized transient EPR spectrum of OEPVO in toluene taken at 80 K during the first 10 μs after the laser flash is shown in the top left part of Figure 2. As can be seen, the spectrum is about 50 mT wide and has only positive intensity; hence, it shows purely absorptive net polarization. However, the assignment of the spectrum to a particular state is not immediately apparent. In principle, it could contain contributions from the trip-doublet, trip-quartet, and/or the ground state depending on the nature of the excited-state dynamics and the values of the magnetic parameters. In the top right part of Figure 2, a representative EPR transient taken at the magnetic field position

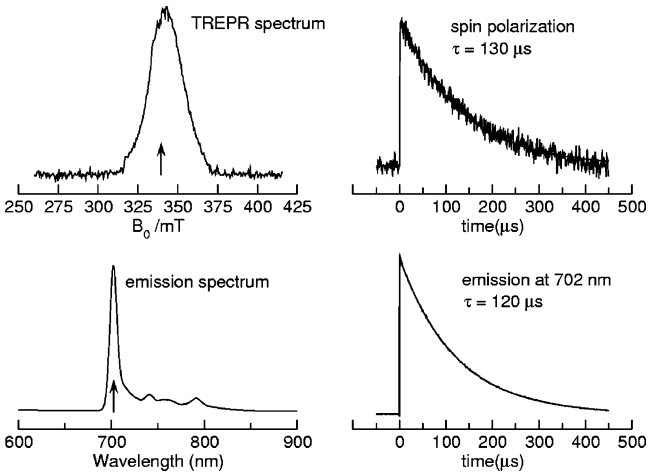

Figure 2. Transient EPR spectrum and spin polarization decay of vanadyl octaethylporphyrin at 80 K (top) compared to the optical emission spectrum and luminescence decay taken at 77 K (bottom). The spin polarization pattern is the transient EPR signal intensity at 5 μs following the laser flash. The spin polarization decay was taken at the field position indicated by the arrow under the spectrum. The luminescence decay was measured at 702 nm, also indicated by an arrow under the emission spectrum. The two decay curves are monoexponential and are governed by approximately the same lifetime as indicated in the figure. In both cases, the excitation wavelength was 532 nm and the solvent was toluene. The sample used for the optical experiments also contained 5% polystyrene (see Materials and Methods).

indicated by the arrow under the TREPR spectrum is shown. The corresponding optical emission spectrum and the decay of the luminescence measured at 702 nm are presented in the bottom part of Figure 2. Fits of the transients using a monoexponential decay function and the lifetimes obtained from the fits are also shown in Figure 2.

As can be seen in Figure 2, the spin polarization and luminescence lifetimes are nearly identical. Previous studies[8,9] of vanadyl and copper (II) porphyrins suggest that the long-lived luminescence arises from radiative decay of the trip-doublet and trip-quartet states following very rapid ISC to the trip-quartet. The fact that the spin polarization has the same lifetime as the luminescence suggests that it is also governed by the lifetimes of the trip-doublet and trip-quartet states. This interpretation implies that either the spin−lattice relaxation time in the excited states must be considerably longer than the lifetime of the states or a spin-selective dynamic process maintains the spin polarization during the lifetime of the excited states. In addition, predominantly multiplet polarization is expected for the trip-quartet if it is populated by spin−orbit coupling-mediated intersystem crossing from the trip-doublet. The fact that the spectrum is dominated by net polarization again suggests the possibility of spin selective excited-state dynamics.

If this is correct, then the spin polarization is likely to be temperature and orientation dependent. Thus, we have taken spectra of OEPVO at 50 K in the liquid crystal E7. It is well-known that when solutes are dissolved in a nematic liquid crystal they are partially ordered by solvent−solute interaction and can be macroscopically oriented in an external magnetic field. If the solution is then frozen in the presence of the field, the orientation is at least partially retained in the resulting solid. In the case of OEPVO, the orientation of the sample can be monitored using the steady-state EPR spectra.

3.2. X-Band Steady-State EPR Spectrum of Vanadyl Octaethylporphyrin. Figure 3 shows experimental (solid lines) and calculated (dashed lines) steady-state X-band EPR spectra

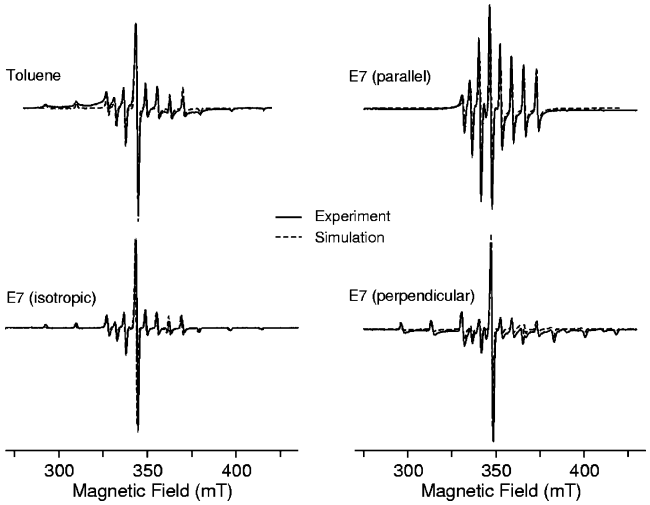

Figure 3. Steady-state EPR spectra of the ground state of vanadyl octaethylporpyrin measured in toluene and the liquid crystal E7 using field modulation. The solid curves are the experimental X-band spectra measured at 50 K. For E7, the three spectra correspond to (i) an isotropic distribution of director orientations relative to the magnetic field (bottom left), (ii) the director oriented parallel to the magnetic field (top right), and (iii) the director oriented perpendicular to the magnetic field (bottom right). The dashed curves are the simulations of the thermal equilibrium spectrum. The g-tensor and hyperfine coupling constants used in the simulation are given in Table 1. For all simulations, the half line width $\Delta = 0.5$ mT and the microwave frequency (expressed in magnetic field units) is $\omega_0 = 350$ mT. The microwave frequency of the experimental spectra is not calibrated. For the partially oriented samples, the order matrix is found to be axially symmetric with $S_{zz} = -0.4$.

of OEPVO at 50 K. Note that these spectra are measured using field modulation and are not spin-polarized. The spectra show sharp peaks due to hyperfine coupling of the unpaired *d*-electron with the $I = 7/2$ vanadium nucleus. The hyperfine couplings to the four nitrogen nuclei[53] are not resolved under the conditions used but contribute to the line width. The eight most prominent peaks arise primarily from the in-plane (*x*,*y*) components of the vanadium hyperfine coupling tensor and have a splitting of roughly 6.0 mT. The out-of-plane (*z*) component has a larger splitting of ~15 mT.[54] As can be seen, only the smaller in-plane splitting is observed when the liquid crystal director is parallel to the field (Figure 3, top right), whereas the large splitting dominates when the director is perpendicular to the field (Figure 3, bottom right). This behavior is expected because the plane of the porphyrin ring is expected to be preferentially oriented along the director of the liquid crystal, i.e., in-plane directions are expected to have positive order parameters.

The g-tensor and vanadium hyperfine coupling tensor used to simulate the spectra are given in Table 1 (ground-state values) and are in good agreement with those found for other vanadyl porphyrins.[54] The nitrogen hyperfine couplings have been taken into account in the inhomogeneous line width. The importance of these simulations, which will be discussed in more detail below, is that they provide independent values for the g-tensor, vanadyl hyperfine tensor and order matrix needed for simulating the transient EPR polarization patterns.

3.3. X-Band Spin-Polarized TREPR Spectra at 50 K. Figures 4, 5, and 6 show spin-polarized transient EPR spectra of OEPVO at X-band measured at 50 K in the liquid crystal E7. In Figure 4, the sample was frozen outside the magnetic field and is not oriented, whereas Figures 5 and 6 are for the director oriented parallel and perpendicular to the field, respectively. Each figure shows two spectra taken at different delay times after the laser flash. In contrast to 80 K (Figure 2), the

TABLE 1: Magnetic Parameters of Vanadyl Octaethylporphyrin

g tensor	g_{xx}	g_{yy}	g_{zz}	
ground state (g_{VO})	1.980	1.980	1.960	E7
	1.980	1.980	1.955	toluene
($\pi-\pi^*$) triplet (g_T)	2.0023	2.0023	2.0023	
trip-quartet $(2/3)g_T + (1/3)g_{VO}$	1.995	1.995	1.988	
vanadium hfc tensor (mT)[a]	A_{xx}	A_{yy}	A_{zz}	
ground state (A_D)	5.80	5.80	17.05	E7
	6.00	6.00	17.10	toluene
zero-field splitting (mT)[a]	*D*	*E*		
trip-quartet	17.5	1.5		
OEPH2[b] triplet state	51	2		
OEPZn[c] triplet state	37	5		

[a] The values in magnetic field units are related to frequency units by $g_e\beta/h = 28.024$ MHz/mT. [b] Free-base octaethylporphyrin. [c] Zinc octaethylporphyrin.

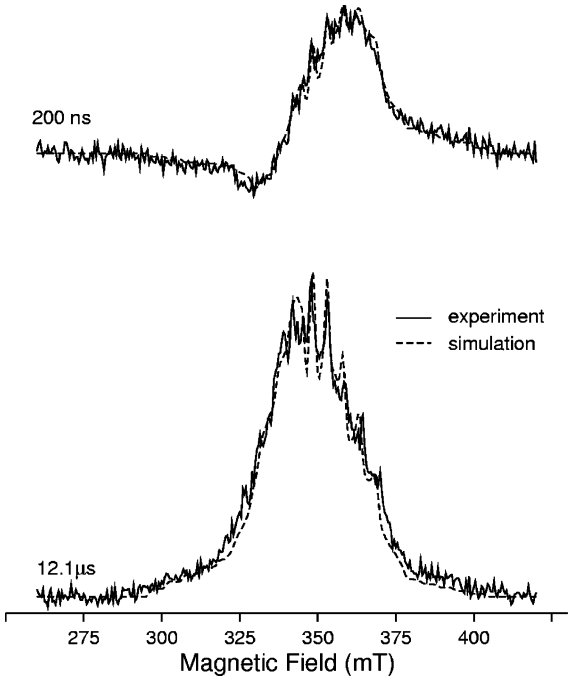

Figure 4. X-band (9 GHz) spin-polarized transient EPR spectra of vanadyl ocaethylporphyin in E7 at early and late delay times following light excitation at 50 K. Early spectrum (top): 100−300 ns. Late spectrum (bottom): 12.0−12.2 μs. The spectra are measured using direct detection, and positive signals represent microwave absorption whereas negative signals are emission. The sample was frozen outside the magnetic field and is not oriented. The dashed line is a simulation, as described in the text, using the magnetic parameters for the trip-quartet, given in Table 1. The calculated spectra are the sum of two multiplet polarization patterns, $\Delta\rho_M^{axial}$ and $\Delta\rho_M^{nonaxial}$, and a net polarization pattern $\Delta\rho_N = \kappa_1\Delta\rho_N(z) + \kappa_2\Delta\rho_N(xy)$. The weights of the three components ($\Delta\rho_M^{axial}$, $\Delta\rho_M^{nonaxial}$, $\Delta\rho_N$) are (0.185, −0.029, 0.189) for the early spectrum and (−0.069, 0.040, 0.545) for the late spectrum. The ratio of the two contributions to the net component is fixed at $\kappa_1/\kappa_2 = 0.473$ for both spectra.

polarization patterns at 50 K (Figures 4, 5, and 6) change significantly with time and show a great deal of structure. In all cases, a multiplet pattern is observed at early time (top spectrum in each figure), whereas at later time, the polarization is purely absorptive (bottom spectrum in each figure) and shows a clear pattern of hyperfine lines near the center of the spectrum. All of these features, the multiplet and net spin polarization and the hyperfine pattern, are strongly orientation dependent.

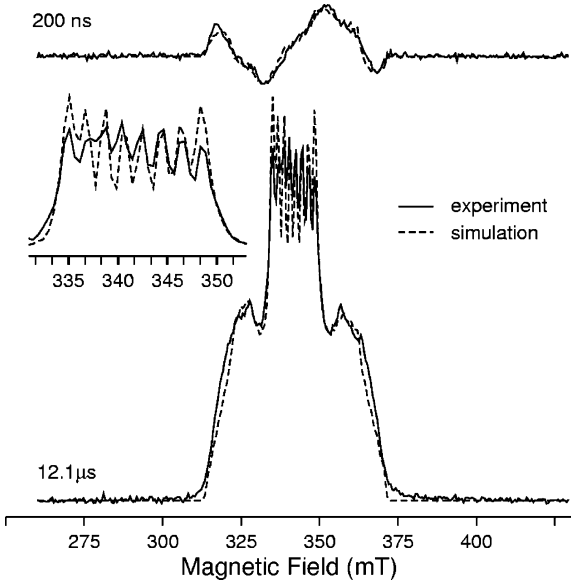

Figure 5. X-band (9 GHz) spin-polarized transient EPR spectra of vanadyl ocaethylporphyin in the liquid crystal E7 with the director oriented parallel to the magnetic field. The spectra are taken under the same conditions and calculated as those shown in Figure 4, except that the orientation distribution described in Appendix 2 has been introduced such that $S_{zz} = -0.4$. The central region of the spectrum at 12.1 μs is also plotted on an expanded to scale to show the hyperfine splitting of the vanadium nucleus more clearly. The weights of the three components ($\Delta\rho_M^{axial}$, $\Delta\rho_M^{nonaxial}$, $\Delta\rho_N$) are (0.074, −0.107, 0.049) for the early spectrum and (−0.026, 0.006, 0.951) for the late spectrum. The ratio of the two contributions to the net component is fixed at $\kappa_1/\kappa_2 = 0.670$ for both spectra.

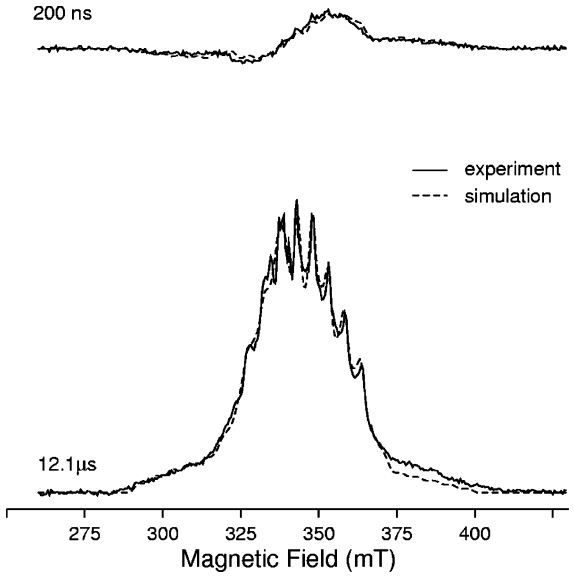

Figure 6. Transient EPR spectra of vanadyl ocaethylporphyin in the liquid crystal E7 corresponding to those in Figure 4 except that the director is oriented perpendicular to the magnetic field. The weights of the three components ($\Delta\rho_M^{axial}$, $\Delta\rho_M^{nonaxial}$, $\Delta\rho_N$) are (0.112, −0.106, 0.067) for the early spectrum and (−0.056, 0.071, 0.958) for the late spectrum. The ratio of the two contributions to the net component is fixed at $\kappa_1/\kappa_2 = 0.653$ for both spectra.

4. Discussion

The observation of an orientation-dependent multiplet pattern suggests that the polarization arises from the trip-quartet state. However, it is useful to first summarize the expected EPR properties of the possible states before making a definitive assignment.

4.1. EPR Properties of Strongly Coupled Triplet−Doublet Spin Systems. If the exchange coupling between the π-electrons and the *d*-electron is much larger than the difference in the precession frequencies of the spins then the three spin states, sing-doublet (ground state), trip-doublet, and trip-quartet, can be treated separately and their spin-Hamiltonians can be written as:

$$H_G = \hbar(\omega_{VO}S_{VOz} + \vec{S}_{VO}\mathbf{A}\vec{I})$$
$$H_D = \hbar(\omega_D S_{Dz} + \vec{S}_D\mathbf{A}_D\vec{I})$$
$$H_Q = \hbar(\omega_Q S_{Qz} + \vec{S}_Q\mathbf{A}_Q\vec{I} + \vec{S}_Q\mathbf{D}_Q\vec{S}_Q) \quad (1)$$

Here we have neglected the Zeeman interaction of the vanadium nucleus, *I*, because it is much weaker than the hyperfine interaction. The values of resonance field positions, $\omega_{D,Q}$, hyperfine interactions $\mathbf{A}_{D,Q}$, and ZFS tensor $\mathbf{D}_Q$ of the trip-doublet and trip-quartet can be related to the corresponding values of the triplet and doublet (see for example ref 55). The values of resonance fields are:

$$\omega_D = 4/3\omega_T - 1/3\omega_{VO}$$
$$\omega_Q = 2/3\omega_T + 1/3\omega_{VO} \quad (2)$$

where

$$\omega_{T,VO} = g_{T,VO}\beta B \quad (3)$$

are the resonance frequencies for the excited triplet of the porphyrin ring, subscript *T*, and doublet unpaired electron of vanadyl, subscript *VO*.

The hyperfine interactions in trip-doublet and trip-quartet states are likewise given by:

$$\mathbf{A}_Q = -\mathbf{A}_D = 1/3\mathbf{A} \quad (4)$$

The spin−spin contribution to the ZFS is given by:[55,56]

$$D = (1/3)D_T + (1/3)D_{TD} \quad (5)$$

where D_T is the ZFS of the triplet and D_{TD} is the dipolar coupling between the triplet and the doublet. These expressions in combination with the expected properties of the spin polarization allow the observed spectra to be assigned.

4.2. Assignment of the Spin Polarization Patterns. The multiplet contribution is most easily explained as being due to the trip-quartet state. A multiplet pattern for trip-doublet or ground doublet state would only be expected if the nuclear spins were involved in the generation of polarization. However, such mechanisms are extremely inefficient if the hyperfine interaction is 3 orders of magnitude smaller than the energy difference between the trip-quartet and trip-doublet. Hence, we assign the multiplet pattern to the trip-quartet. The net polarization pattern can be most easily assigned using the hyperfine couplings. With the director parallel to the field (Figure 5), the in-plane component of the hyperfine tensor dominates, whereas the out-of-plane component is seen with the director perpendicular to the field (Figure 6).

Inspection of the spectra in Figures 5 and 6 shows that the in-plane component of the hyperfine splitting is ∼2 mT (Figure 5) whereas the out-of-plane component is ∼6 mT (Figure 6). From the values of 5.80 and 17.05 mT obtained for the respective components of the vanadyl hyperfine coupling tensor in the ground doublet state, we predict splittings of 1.93 and 5.68 mT, respectively, in the trip-quartet and trip-doublet from eq 4. Hence, the observed splittings in the spectra in Figures

4−6 are in good agreement with those expected for either the trip-quartet or trip-doublet state.

An interesting point in Figures 5 and 6 is that that the ratio of the in-plane and out-of-plane components of the hyperfine tensor is ∼1:3, so that the in-plane component in the ground doublet state has about the same value as the out-of-plane component in the trip-doublet or trip-quartet. Because of this, partially oriented samples are required for an unambiguous assignment of the hyperfine splittings in the spin-polarized spectra. From Figures 5 and 6, it is clear that both components of the hyperfine tensor are reduced by a factor of ∼3 compared to the ground state. The fact that the net polarization pattern is the same width as the multiplet pattern and that the spin polarization has the same lifetime as the luminescence clearly suggests that both polarization patterns arise from the quartet state. To test this assignment, we have simulated the experimental spectra using a model[57,58] we developed recently to describe the polarization generated during intersystem crossing induced by spin−orbit coupling.

4.3. Spectral Simulations. The parameters needed for the simulations are given in Table 1 and have been fixed as far as possible from the ground-state spectra (Figure 3). For all of the calculated spectra shown in Figures 3−6, we use the appropriate static spin Hamiltonian given in eq 1.

4.3.1. Steady-State Spectra. To simulate the steady-state spectra (Figure 3), a Boltzmann population distribution was assumed, and the calculated spectra were convoluted with a Gaussian line shape to take inhomogeneous broadening into account and then differentiated numerically. The hyperfine couplings, g-values, and order parameter were adjusted to obtain the best agreement with the experimental spectra. Compared to the spin-polarized spectra of the quartet state, the ground-state spectra have a broader overall shape due to the larger hyperfine splitting and, thus, are more sensitive to the EPR parameters and the distribution function. Therefore, the g-values and hyperfine coupling parameters shown in Table 1 and the order parameter $S_{zz} = -0.4$ obtained from the fit of the steady-state spectra were kept constant in the simulations of the spin-polarized spectra.

4.3.2. TREPR Spectra: For the simulations of the spin-polarized spectra, we have estimated the Zeeman frequency, ω_Q, and the vanadium hyperfine tensor, **A**, of the trip-quartet from the corresponding values for the ground state and triplet excitation of the porphyrin ring using eqs 2−5. As shown in Table 1, we assume that the triplet excitation has an isotropic g-tensor at the free electron g-value. Note that the g-values and hyperfine couplings of the ground state of vanadyl porphyrin in toluene and in the liquid crystal E7 differ slightly. However, because the ground state values are scaled by a factor of 1/3 when calculating the parameters for the trip-quartet (see eqs 4 and 5), the solvent dependence becomes negligible. Careful comparison of the spin-polarized spectra (Figures 4−6) and ground state spectra (Figure 3) shows that the ratio of the hyperfine splittings deviates slightly from the expected ratio of 1/3 as given by eq 4. The splittings in the polarization pattern were found to be about 5% smaller than expected (see Table 1). This deviation is likely the result of a slight difference in the spin density distribution of the *d*-electron in the ground state and the excited state.

The zero-field splitting parameters were estimated initially by visual inspection of the spectra and then fitted to the experimental spectra (see below). The values of $D = 17.5$ mT and $E = 1.5$ mT reported in Table 1 gave the best agreement with experiment. The polarization patterns are very sensitive to these values, and the error is estimated to be less than 1 mT.

4.3.3. Spin Polarization and Fitting Procedure. In the TREPR technique, the signal is proportional to the light-induced polarization after the laser flash. This is in contrast to steady-state EPR observations where the signal is proportional to the Boltzmann polarization at thermal equilibrium. So, for the TREPR spectra, the spin polarization must also be taken into account. Here, we express the polarization as the traceless diagonal part of the reduced density matrix for the quartet state. In general, it may be written as the sum of multiplet and net contributions, which we label $\Delta\rho_M$ and $\Delta\rho_N$, respectively. We expect the trip-quartet to be populated initially by ISC from the trip-doublet (see Figure 1). This process will be governed by spin−orbit coupling,[57,58] which follows the molecular symmetry. Hence, the polarization can be broken up into terms associated with each of the molecular axes. For porphyrins, spin−orbit coupling is expected to be most effective about the molecular *z*-axis. However, contributions associated with the molecular *x*- and *y*-axes may also be involved. The mutliplet polarization, $\Delta\rho_M$, can be described by the even powers of the spin operators, and because it reflects the traceless anisotropy of the spin−orbit coupling, we need only introduce two contributions: (i) an axial term describing the contribution associated with the *z*-axis, which is proportional to $S_{\Omega,Qz}^2 - 1/3\vec{S}_Q^2$ in the molecular frame, Ω, and (ii) a nonaxial term describing the difference of contributions about the molecular *x*- and *y*-axes, which is proportional to $S_{\Omega,Qx}^2 - S_Q^2$. Transforming to the laboratory frame and ignoring off-diagonal elements gives:

$$\Delta\rho_M^{\text{axial}} \propto (1 - 3\cos^2\theta)(S_{\Omega,Qz}{}^2 - 1/3\vec{S}_Q{}^2)$$
$$\Delta\rho_M^{\text{nonaxial}} \propto \sin^2\theta\cos 2\phi(S_{\Omega,Qz}{}^2 - 1/3\vec{S}_Q{}^2) \quad (6)$$

where θ and ϕ describe the orientation of the porphyrin molecule along the external field.

The net polarization is described by the odd powers of the spin operators,[57,58] and in principle, a term for each of the components of the spin−orbit coupling should be introduced. In practice, however, the deviation from axial symmetry is very small and the linear and cubic terms are virtually indistinguishable. Therefore, to reduce the number of independent contributions as far as possible, we use only the linear terms and combine the contributions from the *x*- and *y*-directions into a single term. This gives:

$$\Delta\rho_N(z) \propto \sin^2\theta\, S_{Qz}$$
$$\Delta\rho_N(xy) \propto \cos^2\theta\, S_{Qz} \quad (7)$$

Taking the amplitudes of these four contributions as adjustable parameters, we have fit the experimental TREPR spectra as follows. First, all four contributions were adjusted independently to reproduce the experimental spectrum summed over a series of 200 ns time windows chosen to span the time region during which the multiplet polarization evolves to net polarization. The ratio between the two net contributions was then held fixed at the value obtained, and all other time windows in the dataset were fit using two independent multiplet patterns and one net contribution representing the two net patterns with fixed ratio. The results of the fits for two selected time windows are shown as dashed curves in Figures 4−6.

As can be seen in Figures 4−6, excellent agreement between the simulated and experimental spectra is obtained. This clearly

identifies the trip-quartet state as the origin of both the multiplet pattern at early time and the net polarization pattern at late time. (The ratios of the two net contributions are given in the figure captions). It was found that the inhomogeneous Gaussian linewidths of the TREPR spectra were noticeably larger than those of the corresponding steady-state EPR spectra. It is likely that this difference reflects the excited-state dynamics that also lead to the evolution from a multiplet pattern at early time to the net pattern at late time.

4.4. Temperature Dependence of the Spin Polarization Decay. On the basis of the above assignment, we can draw two important conclusions: (i) The quartet state spin polarization changes from an initial multiplet pattern to a net absorptive pattern at later time. (ii) The decay of net polarization and the luminescence are governed by the lifetime of the trip-quartet. We propose that the evolution of the spin polarization is the result of transitions between the trip-quartet and trip-doublet as thermal equilibration occurs, and a detailed model for this process is developed in the accompanying paper.[49] As a first step in this analysis, we examine the temperature dependence of the trip-quartet lifetime evaluated from the decay rate of the net polarization.

Generally, when electronic relaxation from the trip-quartet state takes place both as decay from the thermally repopulated trip-doublet state and direct relaxation from the trip-quartet state, the lifetimes of the excited states are determined by the relaxation rates of the two excited states and by the energy gap.[8,9,21] Whether the trip-doublet and trip-quartet states are in thermal equilibrium or not depends on temperature region as well as the relaxation rates and the energy gap.

From previous studies[8,21,59] of vanadyl porphyrins, it is not clear whether thermal equilibrium between the trip-doublet and trip-quartet states is established at low temperatures. In addition, it is difficult to tell that the observed emission of OEPVO is only from the trip-doublet state, or from both the trip-doublet and trip-quartet as observed[9] in OEPCu, which is suggested[8,9] to have a larger energy gap than OEPVO. However, because the spin-polarization decay rate of the trip-quartet state and emission decay rate are identical at 77 K as in Figure 2, we can safely assume that the lifetime of the net polarization and luminescence both represent the lifetime of the trip-quartet state. Here, we analyze the temperature dependence of the polarization decay and discuss the electronic dynamics to confirm the proposed kinetic scheme, on which our spin-polarization model presented in the following paper is based. Because the expressions for the decay rates are quite complicated for a completely general kinetic scheme,[9] we simplify the analysis by assuming thermal equilibrium between the trip-quartet and trip-doublet.

With this assumption, the lifetime can be written in a straightforward manner based on the two-state model proposed by Gouterman et al.[8] and expanded upon by Asano et al.[9] In this model, the trip-doublet and trip-quartet states are separated by an energy gap ΔE_{DQ} and have decay rates k_{DG} and k_{QG} to the ground state, respectively (see Figure 1). The lifetime of the trip-quartet in thermal equilibrium is given by:[9]

$$\tau = \frac{1 + K}{k_{DG}K + k_{QG}} \tag{8}$$

where $K = 1/2 \exp\{-\Delta E_{DQ}/k_B T\}$ is the equilibrium constant between the trip-doublet and trip-quartet states.

Figure 7 shows the experimental lifetimes of the net polarization (●) and the optical emission (□,■) of OEPVO as a function of temperature. Also shown are the luminescence lifetimes of vanadyl etioporphyrin (EtioVO) taken from the literature[8] (○).

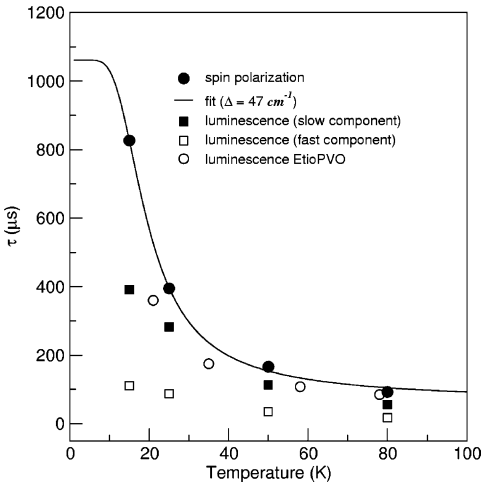

Figure 7. Temperature dependence of the spin polarization lifetime of OEPVO in E7. (●) Experimental values of the spin polarization lifetime, *t*, at each temperature. The solid curve is a fit to the experimental transient EPR data using eq 8, which describes the observed decay of the trip-quartet via the scheme shown in Figure 1. The fit yields values of 47 cm^{-1} for ΔE_{DQ}, 20 μs for k_{DG}^{-1}, and 1.06 ms for k_{QG}^{-1}. The squares are luminescence decay lifetimes for OEPVO in a PMMA film. The decays are found to be biexponential and ■ and □ are the two decay components. The luminescence decays were taken at 696 nm, and the excitation wavelength was 532 nm for both the EPR and optical emission measurements. (○) Luminescence lifetimes for vanadyl etioporphyrin in PMMA taken from ref 8.

Clearly, the temperature dependences of the spin polarization and luminescence decays are very similar. However, the spin polarization lifetimes are slightly longer than the luminescence lifetimes at all temperatures. This difference is probably because the luminescence was measured in PMMA whereas the spin polarization decays were taken in E7. The optical emission decay for OEPVO was found to be biphasic, and the filled and open squares are the two decay components. For the spin polarization decays, the signal-to-noise ratio was not sufficient to clearly distinguish between monoexponential or biexponential behavior. Therefore, only a single lifetime is given. The ratio of the amplitudes and the ratio of the lifetimes of the two kinetic components obtained from the optical data are both independent of temperature. This finding suggests that they arise from different local environments rather than from competing processes within the molecule. Also shown in the Figure 7 is a fit of eq 8 to the spin polarization decay lifetimes. The fit yields a value of 47 cm^{-1} for ΔE_{DQ}, 20 μs for k_{DG}^{-1}, and 1.06 ms for k_{QG}^{-1}. These values are in line with what one would expect and are similar to those obtained from other related porphyrins.[8,9] The value of 47 cm^{-1} for ΔE_{DQ} is almost identical to that reported for EtioVO[8,9] (40 cm^{-1}) but is considerably smaller than the value ~500 cm^{-1} suggested for vanadyl tetraphenylporphyrin (TPPVO).[21] This result is reasonable because the $^3(\pi,\pi^*)$ excitation involved in the lowest trip-doublet and trip-quartet states of OEPVO and EtioVO have the same $^3(a_{1u}e_g)$ electronic configuration, whereas for TPPVO, the configuration is $^3(a_{2u}e_g)$.[9,14]

In eq 8, it assumed that the establishment of equilibrium is fast compared to the two decay rates. Because the fit gives only *K*, the ratio of the rates of the back-and-forth transitions between the trip-doublet and trip-quartet, it is important to consider whether this assumption is valid. The lifetime associated with ISC from the trip-doublet to trip-quartet probably lies in the range of a few picoseconds.[9,17] However, even if we assume that it is as long as ~1 ns, the lifetime for the reverse process, i.e., from the trip-quartet to the trip-doublet, is calculated as

ca. 200 ns at 15 K with a 47 cm^{-1} gap. These values are sufficiently short that despite the uncertainty in the ISC rates, it is clear that thermal equilibrium between the trip-doublet and trip-quartet states is established during the excited-state lifetime. Thus, we can conclude that the luminescence and spin polarization decay under thermal equilibration between the trip-doublet and trip-quartet states even at temperatures as low as 15 K. We also note that with a 47 cm^{-1} gap, it is very difficult to distinguish between emission from the trip-quartet and trip-doublet on the basis of the emitted wavelength because the energy corresponds to only 2 nm.

The value of ΔE_{DQ} for OEPVO is significantly smaller than that obtained for OEPCu.[8] This result is consistent with what is expected for the difference of the exchange interaction between OEPCu and OEPVO; the vanadium(IV) ion has an unpaired *d* electron mainly in d_{xy} orbital, whereas for the copper(II) ion, the unpaired electron resides in a $d_{x^2-y^2}$ orbital, which is expected to overlap to a greater extent with the porphyrin π-electron system.

4.5. Magnetic Parameters of the Trip-Quartet State. The data in Table 1 give a more detailed picture of the magnetic interaction parameters of a porphyrin trip-quartet than has previously been available. The slight deviation of the hyperfine couplings from the value predicted by eq 4 discussed above indicates that the spin density at the vanadium nucleus in quartet state is lower than in the ground state. One possible explanation for this observation is that the vanadyl d_{xy} orbital may be mixed differently with the π-orbitals of the porphyrin in the excited state compared to the ground-state, resulting in a lower spin density at the vanadium nucleus.

One of the most striking features of the trip-quartet is that the ZFS parameters are of similar magnitude to those of the triplet state of free-base, Zn, and Mg porphryins.[16] The values measured for free base and Zn analogues of OEPVO are given in Table 1 for comparison. In general, the zero-field splitting (ZFS) contains contributions from the direct spin−spin dipolar coupling as well as from the spin−orbit coupling. In the triplet states of organic compounds with extended π-systems,[60] the direct spin−spin coupling usually dominates. In the diamagnetic metalloporphyrins, both contributions play a role, but the contribution from spin−orbit coupling varies strongly depending on the metal. For the diamagnetic metals of the first transition period, the spin−orbit contribution is much smaller than the spin−spin contribution. For the metals further down the period table such as Pd, the spin−orbit contribution dominates. Corresponding data for the excited multiplet states of porphyrins with paramagnetic metals are scarce. However, copper porphyrins have ZFS ($|D| \sim 370$ mT (0.35 cm^{-1}) and $|E| = \sim 290$ mT (0.27 cm^{-1}))[22] that are about an order of magnitude larger than found, here, for OEPVO. Thus, it would appear that there is likely a large difference in the spin−orbit contribution to the ZFS in OEPVO and copper porphyrins.

Another important aspect of the results is that the observed spin polarization is very different from that found for similar compounds such as copper porphyrins[24] and a chromium(V) oxide corrole.[26] In both of these cases, emissive polarization of the ground state was observed but no signals from the quartet state were detected. There are a number of reasons for this observation. First, the larger ZFS of the copper porphyrins makes observation of the quartet spin polarization difficult. Second, luminescence data for these and other related compounds[8,9,59,61] point toward population of the trip-quartet at low temperature but quenching at high temperature. Thus, at the high temperatures under which chromium(V) oxide corrole[26] was measured, the lifetime of the excited states is probably too short for them to be detected by TREPR.

5. Concluding Remarks

With the analysis of the spin polarization patterns of OEPVO presented here, we have established that they arise from the trip-quartet state. The evolution of the spin polarization with time therefore reflects the dynamics of the trip-quartet. In the accompanying paper[49] we will explore these dynamics in more detail and present a model based on thermal equilibrium between the trip-doublet and trip-quartet to explain the evolution of the spin polarization.

Acknowledgment. This work was supported by the Natural Sciences and Engineering Research Council (NSERC) and by two Grants-In-Aid for Scientific Research from JSPS, No. 11694061: (International Joint Research, B) and No. 16550009.

Appendix 1: Calculation of the EPR Spectra

The frequencies of the EPR transitions at a fixed value of the external magnetic field are calculated as the differences between two eigenvalues of the spin Hamiltonian (eq A1.1). In rotating frame with ω_0 as the microwave frequency thus gives:

$$\Delta\omega_{ij} = \tilde{H}_{Q,ii} - \tilde{H}_{Q,jj} - \omega_0 \qquad \text{(A1.1)}$$

where the symbol "$\sim$" is used to refer to the representation of the operator in the frame in which the spin-Hamiltonian is diagonal, and *i* and *j* denote the two spin eigenstates. The intensity of the stick spectrum at position *B* with step ΔB is then described as

$$I_B \sim \sum_{ij} |\tilde{S}_x|^2_{ij} (\tilde{\rho}_{ii} - \tilde{\rho}_{jj}) U(\Delta\omega_{ij}) \qquad \text{(A1.2)}$$

The operator ρ describes the density matrix and the function *U* is nonzero only if $\Delta\omega_{ij}$ changes sign in the interval $(B, B + \Delta B)$:

$$U(x) = \begin{bmatrix} 1 & x_B x_{B+\Delta B} < 0 \\ 1/2 & x_B x_{B+\Delta B} = 0 \\ 0 & x_B x_{B+\Delta B} > 0 \end{bmatrix}$$

The intensity function runs all values of the external field and is summed over all possible orientations of the molecule relative to the field. Because of the conditions under which the EPR signal is observed, it is invariant to rotations about the external field $\vec{e}_B = \vec{e}_B(\theta,\varphi)$, and only two angles are required to fix the vector $\vec{e}_B$ in the molecular frame. The orientations of $\vec{e}_B$ map out points on the surface of a sphere, and the algorithm should distribute the points quasi-uniformly over the surface. Because the spectrum does not depend on the sign of $\vec{e}_B$ the calculation can be restricted to a hemisphere. A uniform distribution can be achieved by choosing points on a spiral that runs from the equator to the pole in such a way that the angle between any pair of neighboring points is constant. This method was first suggested by Mombourquette and Weil[62] who computed the values of θ_i and φ_i numerically. Later Ponti[52] derived the following simple analytical expressions (note that the expressions in Ponti[52] are in error by a factor of 2), which give a distribution of points of similar uniformity:

$$\begin{bmatrix} \theta_i = \arccos(i - 1/2/n) \\ \varphi_i = \sqrt{2\pi n}\arcsin(i - 1/2/n) \end{bmatrix} i = 1 \cdots n \qquad \text{(A1.3)}$$

where n is the number of points on the hemisphere, and i is an iterator running from 1 to n.

Appendix 2: Calculation of the Orientation Distribution

To describe the partially oriented samples in E7, the stick spectrum for each orientation is given a weighting factor determined by the orientation distribution function:

$$f(\Omega) \propto \exp(-V(\Omega)/kT) \tag{A2.1}$$

where Ω, represents the set of angles describing the orientation and $f(\Omega)$ is the probability of the orientation. $V(\Omega)$ represents the potential energy of a given orientation. The most general form for $V(\Omega)$, consistent with the known properties of liquid crystals, is the product of two second-rank tensors, one describing the solvent and the other the solute.[46,63−66] In a space-fixed axis system, the potential can then be written as:

$$V(\Omega) = -1/2\sum_{IJ} F_{IJ}T_{IJ} \tag{A2.2}$$

where F is a traceless tensor representing the liquid crystal and T is the molecular property of the solute that interacts with F. I and J denote the space-fixed axes. In a nematic liquid crystal such as E7, F is axially symmetric and diagonal if one of the space-fixed axes (usually defined as Z) is parallel to the director. Thus, $V(\Omega)$ can be written as a function of F_{ZZ} and the orientation of the director in the principal axes of T.

$$\begin{aligned} V &= -(1/2)F_{ZZ}\sum_{k} T_{kk}((3/2)\cos^2\theta_{kZ} - (1/2)) \\ &= a((3/2)\cos^2\beta - (1/2)) + b\sin^2\beta\cos 2\alpha \end{aligned} \tag{A2.3}$$

where the parameters a and b describe the strength of the interaction between the porphyrin and the liquid crystal and the angles α and β define the orientation of the molecule relative to the director of the liquid crystal. The distribution function also determines the Saupe order matrix, S, which is diagonal in the principal axes of T and has two independent nonzero elements:

$$\begin{aligned} S_{zz} &= \langle(3/2)\cos^2\beta - (1/2)\rangle \\ (S_{xx} - S_{yy}) &= \langle(3/2)\sin^2\beta\cos 2\alpha\rangle \end{aligned} \tag{A2.4}$$

The angular brackets denote the ensemble average. For OEPVO, the 4-fold rotational symmetry also requires that the parameter b in the potential and $(S_{xx} - S_{yy})$ are zero.[64] This requirement is confirmed by our simulations, which give the best fit for $b = 0$. Hence, the potential contains a single unknown parameter, a, and the orientation distribution is characterized by a single order parameter, S_{zz}. The symmetry also requires that the principal axes of the magnetic interaction tensors and the order matrix are the same.

For samples in which the director is parallel to the magnetic field, the orientation of the molecular axes relative to the magnetic field and to the director can be described by the same two angles, i.e., $\beta = \theta$ and $\alpha = \phi$. In the more general case when the director and the magnetic field are not parallel, a transformation between the two sets of angles is required and the probability function takes the form:

$$f_{\psi,\chi}(\theta,\phi) \propto \exp(-V(\beta,\alpha)/kT) \tag{A2.5}$$

where the angles α and β describing the orientation of the molecule relative to the director can also be expressed as a function of the orientation of the magnetic field in the molecular frame $\vec{e}_B = \vec{e}_B(\theta,\varphi)$, the angle ψ between the magnetic field and the director, and the angle χ that fixes the x-axis of the laboratory frame relative to the director:

$$(\sin\beta\cos\alpha, \sin\beta\sin\alpha, \cos\beta) = (0,0,1)\cdot R_y(\psi)\cdot R_z(\chi)\cdot R_x(\theta)\cdot R_z(\varphi) \tag{A2.6}$$

Here, we use the symbol R to denote the Euler rotation operator. The expansion of equations is

$$\begin{aligned} \sin\beta\cos\alpha &= \sin\theta\cos\varphi, \cos\psi + (\cos\theta\cos\varphi\cos\chi - \sin\varphi\sin\chi)\sin\psi \\ \sin\beta\sin\alpha &= \sin\theta\sin\varphi, \cos\psi + (\cos\theta\sin\varphi\cos\chi + \sin\varphi\sin\chi)\sin\psi \\ \cos\beta &= \cos\theta\cos\psi - \sin\theta\sin\psi\cos\psi \end{aligned} \tag{A2.7}$$

If the EPR signal represents the magnetization along the field, the laboratory frame can be assumed to be axially symmetric, and the orientational distribution is proportional to the integral of equation over the values $0 \le \chi < 2\pi$. Taking the axial symmetry of the OEPVO distribution around the director into account, the orientational distribution for an arbitrary angle ψ between the director and the field is:

$$\begin{aligned} f_{\psi}(\theta) &\propto \exp\{-a(3\cos^2\beta - 1)/kT\} \\ &= \int_0^{2\pi}\exp\{-a(3(\cos\theta\cos\psi - \sin\theta\sin\psi\cos\chi)^2 - 1)/kT\}\,d\chi \end{aligned} \tag{A2.8}$$

These equations are simplified further for the parallel and perpendicular orientations.

$$\begin{aligned} f_{\parallel}(\theta) &\propto \exp -\eta(3\cos^2\theta - 1) \\ f_{\perp}(\theta) &\propto \int_0^{2\pi}\exp\{-\eta(3\sin^2\theta\cos^2\chi - 1)\}\,d\chi \end{aligned} \tag{A2.9}$$

Here we have replaced a/kT with a temperature-independent parameter η to reflect the fact that in the frozen liquid crystal, the reorientation of the solvent and solute are hindered and, hence, the ordering is not expected to vary with temperature.

References and Notes

(1) Straight, S. D.; Andreasson, J.; Kodis, G.; Moore, A. L.; Moore, T. A.; Gust, D. *J. Am. Chem. Soc.* **2005**, *127*, 2717.

(2) Di Valentin, M.; Bisol, A.; Agostini, G.; Fuhs, M.; Liddell, P. A.; Moore, A. L.; Moore, T. A.; Gust, D.; Carbonera, D. *J. Am. Chem. Soc.* **2004**, *126*, 17074.

(3) Kurreck, J.; Niethammer, D.; Kurreck, H. *Chem. Unserer Zeit* **1999**, *33*, 72.

(4) Senge, M. O.; Rossler, B.; von Gersdorff, J.; Schafer, A.; Kurreck, H. *Tetrahedron Lett.* **2004**, *45*, 3363.

(5) Splan, K. E.; Keefe, M. H.; Massari, A. M.; Walters, K. A.; Hupp, J. T. *Inorg. Chem.* **2002**, *41*, 619.

(6) Tomizaki, K.; Loewe, R. S.; Kirmaier, C.; Schwartz, J. K.; Retsek, J. L.; Bocian, D. F.; Holten, D.; Lindsey, J. S. *J. Org. Chem.* **2002**, *67*, 6519.

(7) Ake, R. L.; Gouterman, M. *Theor. Chim. Acta* **1969**, *15*, 20.

(8) Gouterman M.; Mathies, R. A.; Smith, B. E.; Caughey, W. S. *J. Chem. Phys.* **1970**, *52*, 3795.

(9) Asano, M.; Kaizu, Y.; Kobayashi, N. *J. Chem. Phys.* **1988**, *89*, 6567.

(10) Smith, B. E.; M, G. *Chem. Phys. Lett.* **1968**, *2*, 517.

(11) van Dorp, W. G.; Canters, G. W.; van der Waals, J. H. *Chem. Phys. Lett.* **1975**, *35*, 450.

(12) Noort, M.; Jansen, G.; Canters, G. W.; Vanderwaals, J. H. *Spectrochim. Acta, Part A* **1976**, *32*, 1371.
(13) Evans, J. S.; Musselman, R. L. *Inorg. Chem.* **2004**, *43*, 5613.
(14) Gruhn, N. E.; Lichtenberger, D. L.; Ogura, H.; Walker, F. A. *Inorg. Chem.* **1999**, *38*, 4023.
(15) Gouterman, M. Optical Spectra and Electronic Structure of Porphyrins and Related Rings. In *The Porphyrins*; Dolphin, D., Ed.; Academic Press: New York, 1978; Vol. III, p 1.
(16) van der Waals, J. H.; van Dorp, W. G.; Schaafsma, T. J. Electron Spin Resonance of Porphyrin Excited States. In *The Porphyrins*; Dolphin, D., Ed.; Academic Press: New York, 1979; Vol. IV, p 257.
(17) Kobayashi, T.; Huppert, D.; Straub, K. D.; Rentzepis, P. M. *J. Chem. Phys.* **1979**, *70*, 1720.
(18) Kim, D.; Holten, D.; Gouterman, M. *J. Am. Chem. Soc.* **1984**, *106*, 2793.
(19) Rodriguez, J.; Kirmaier, C.; Holten, D. *J. Am. Chem. Soc.* **1989**, *111*, 6500.
(20) Yan, X.; Holten, D. *J. Phys. Chem.* **1988**, *92*, 5982.
(21) Jeoung, S. C.; Kim, D.; Hahn, S. J.; Ryu, S. Y.; Yoon, M. *J. Phys. Chem. A* **1998**, *102*, 315.
(22) van der Poel, W.; Nuijs, A. M.; van der Waals, J. H. *J. Phys. Chem.* **1986**, *90*, 1537.
(23) Yamauchi, S. *Bull. Chem. Soc. Jpn.* **2004**, *77*, 1255.
(24) Rozenshtein, V.; Berg, A.; Levanon, H.; Krueger, U.; Stehlik, D.; Kandrashkin, Y.; van der Est, A. *Isr. J. Chem.* **2003**, *43*, 373.
(25) Hugerat, M.; A. van der Est; E. Ojadi; L. Biczok; H. Linschitz; Levanon, H.; Stehlik, D. *J. Phys. Chem.* **1996**, *100*, 495.
(26) Stavitski, E.; Berg, A.; Ganguly, T.; Mahammed, A.; Gross, Z.; Levanon, H. *J. Am. Chem. Soc.* **2004**, *126*, 6886.
(27) Corvaja, C.; Maggini, M.; Prato, M.; Scorrano, G.; Venzin, M. *J. Am. Chem. Soc.* **1995**, *117*, 8857.
(28) Fujisawa, J.; Ishii, K.; Ohba, Y.; Yamauchi, S.; Fuhs, M.; Mobius, K. *J. Phys. Chem. A* **1997**, *101*, 5869.
(29) Mizuochi, N.; Ohba, Y.; Yamauchi, S. *J. Phys. Chem. A* **1997**, *101*, 5966.
(30) Ishii, K.; Hirose, Y.; Kobayashi, N. *J. Am. Chem. Soc.* **1998**, *120*, 10551.
(31) Fujisawa, J.; Ishii, K.; Ohba, Y.; Yamauchi, S.; Fuhs, M.; Mobius, K. *J. Phys. Chem. A* **1999**, *103*, 3138.
(32) Mizuochi, N.; Ohba, Y.; Yamauchi, S. *J. Chem. Phys.* **1999**, *111*, 3479.
(33) Mizuochi, N.; Ohba, Y.; Yamauchi, S. *J. Phys. Chem. A* **1999**, *103*, 7749.
(34) Conti, F.; Corvaja, C.; Toffoletti, A.; Mizuochi, N.; Ohba, Y.; Yamauchi, S.; Maggini, M. *J. Phys. Chem. A* **2000**, *104*, 4962.
(35) Teki, Y.; Miyamoto, S.; Iimura, K.; Nakatsuji, M.; Miura, Y. *J. Am. Chem. Soc.* **2000**, *122*, 984.
(36) Teki, Y. *Polyhedron* **2001**, *20*, 1163.
(37) Teki, Y.; Miyamoto, S.; Nakatsuji, M.; Miura, Y. *J. Am. Chem. Soc.* **2001**, *123*, 294.
(38) Teki, Y.; Nakatsuji, M.; Miura, Y. *Int. J. Mod. Phys. B* **2001**, *15*, 4029.
(39) Sartori, E.; Toffoletti, A.; Corvaja, C.; Garlaschelli, L. *J. Phys. Chem. A* **2001**, *105*, 10776.
(40) Sartori, E.; Garlaschelli, L.; Toffoletti, A.; Corvaja, C.; Maggini, M.; Scorrano, G. *Chem. Commun.* **2001**, *4*, 311.
(41) Ishii, K.; Ishizaki, T.; Kobayashi, N. *J. Chem. Soc., Dalton Trans.* **2001**, 3227.
(42) Ishii, K.; Hirose, Y.; Fujitsuka, H.; Ito, O.; Kobayashi, N. *J. Am. Chem. Soc.* **2001**, *123*, 702.
(43) Ishii, K.; Bottle, S. E.; Shimizu, S.; Smith, C. D.; Kobayashi, N. *Chem. Phys. Lett.* **2003**, *370*, 94.
(44) Franco, L.; Mazzoni, M.; Corvaja, C.; Gubskaya, V. P.; Berezhnaya, L. S.; Nuretdinov, I. A. *Chem. Commun.* **2005**, 2128.
(45) Asano-Someda, M.; van der Est, A.; Krüger, U.; Stehlik, D.; Kaizu, Y.; Levanon, H. *J. Phys. Chem. A* **1999**, *103*, 6704.
(46) van der Est, A.; Asano-Someda, M.; Ragogna, P.; Kaizu, Y. *J. Phys. Chem. A* **2002**, *106*, 8531.
(47) Asano-Someda, M.; Toyama, N.; Kaizu, Y. *Appl. Magn. Reson.* **2003**, *23*, 393.
(48) Kandrashkin, Y. E.; Asano, M. S.; van der Est, A. *Phys. Chem. Chem. Phys.* **2006**, *8*, 2129−2132.
(49) Kandrashkin, Y. E.; Asano, M. S.; van der Est, A. *J. Phys. Chem. A* **2006**, *110*, 9617.
(50) Stehlik, D.; Bock, C. H.; Thurnauer, M. C. Transient EPR−Spectroscopy of Photoinduced Electronic Spin States in Rigid Matrixes. In *Advanced EPR in Biology and Biochemistry*; Hoff, A. J., Ed.; Elsevier: Amsterdam, 1989; p 371.
(51) van der Est, A.; Hager-Braun, C.; Leibl, W.; Hauska, G.; Stehlik, D. *Biochim. Biophys. Acta* **1998**, *1409*, 87.
(52) Ponti, A. *J. Magn. Res.* **1999**, *138*, 288.
(53) Sato, M.; Kwan, T. *Bull. Chem. Soc. Jpn.* **1974**, *47*, 1353.
(54) Lin, W. C. Electron Spin Resonance and Electronic Structure of Metalloporphyrins. In *The Porphyrins*; Dolphin, D., Ed.; Academic Press: New York, 1979; Vol. IV, p 355.
(55) Bencini, A.; Gatteschi, D. *EPR of Exchange Coupled Systems*; Springer-Verlag: Berlin, 1990.
(56) Boca, R. *Coord. Chem. Rev.* **2004**, *248*, 757−815.
(57) Kandrashkin, Y. E.; van der Est, A. *J. Chem. Phys.* **2004**, *120*, 4790.
(58) Kandrashkin, Y. E.; van der Est, A. *Chem. Phys. Lett.* **2003**, *379*, 574.
(59) Harima, Y.; Kodaka, T.; Kunugi, Y.; Yamashita, K.; Akimoto, Y.; Fujiwara, Y.; Tanimoto, Y. *Chem. Phys. Lett.* **1997**, *267*, 481.
(60) Kay, C. W. M. *J. Am. Chem. Soc.* **2003**, *125*, 13861.
(61) Vitols, S. E.; Friesen, D. A.; Williams, D. S.; Melamed, D.; Spiro, T. G. *J. Phys. Chem.* **1996**, *100*, 207.
(62) Mombourquette, M. J.; Weil, J. A. *J. Magn. Res.* **1992**, *99*, 37.
(63) de Lange, C. A.; Snijders, J. G.; Burnell, E. E. On the orientation of small molecules in anisotropic solvents. In *Nuclear Magnetic Resonance of Liquid Crystals*; Emsley, J. W., Ed.; D. Reidel: Dordrecht, The Netherlands, 1985; p 181.
(64) *NMR of Ordered Liquids*; Burnell, E. E.; de Lange, C. A., Eds.; Kluwer Academic Publishers: Dordrecht, The Netherlands, 2003.
(65) Snijders, J. G.; de Lange, C. A.; Burnell, E. E. *Isr. J. Chem.* **1983**, *23*, 269.
(66) Burnell, E. E.; de Lange, C. A.; Snijders, J. G. *Phys. Rev. A: At., Mol., Opt. Phys.* **1982**, *25*, 2339.